Tectonic implications of Mars crustal magnetism

J. E. P. Connerney*†, M. H. Acuña*, N. F. Ness†‡, G. Kletetschka*§, D. L. Mitchell¶, R. P. Lin¶, and H. Reme‖

*National Aeronautics and Space Administration Goddard Space Flight Center, Greenbelt, MD 20771; ‡University of Delaware, Newark, DE 19716; ¶University of California, Berkeley, CA 94720; §Catholic University of America, Washington, DC 20064; and ‖Centre d'Etude Spatiale des Rayonnements, 31028 Toulouse Cedex 4, France

Mars currently has no global magnetic field of internal origin but must have had one in the past, when the crust acquired intense magnetization, presumably by cooling in the presence of an Earth-like magnetic field (thermoremanent magnetization). A new map of the magnetic field of Mars, compiled by using measurements acquired at an ≈400-km mapping altitude by the Mars Global Surveyor spacecraft, is presented here. The increased spatial resolution and sensitivity of this map provide new insight into the origin and evolution of the Mars crust. Variations in the crustal magnetic field appear in association with major faults, some previously identified in imagery and topography (Cerberus Rupes and Valles Marineris). Two parallel great faults are identified in Terra Meridiani by offset magnetic field contours. They appear similar to transform faults that occur in oceanic crust on Earth, and support the notion that the Mars crust formed during an early era of plate tectonics.

magnetic | planetary | plate tectonics

Precisely how the Mars crust acquired its magnetic imprint is a matter of great interest with far reaching implications for crustal formation and the thermal evolution of Mars. Connerney *et al.* (1) showed that magnetic lineations in the southern highlands could be represented by a pattern of quasi-parallel bands of uniformly magnetized crust with alternating positive and negative polarity. This pattern of magnetization is reminiscent of the alternating magnetic polarities observed over mid ocean ridges on Earth (2) where crustal spreading in the presence of a reversing dynamo creates multiple parallel bands of normal and reversed magnetization aligned with the ridge axis. They suggested that the Mars crust might have formed by a similar process during an early era of plate tectonics, retaining, in places, the magnetic imprint acquired when it formed, billions of years ago. On Earth, this process yields a pattern of magnetization with symmetry about the ridge axis, and adjoining plates are bounded by a unique type of fault ("transform fault"). Neither had been observed on Mars.

Mapping Observations

The magnetic field experiment (3) aboard Mars Global Surveyor (MGS) provides measurements of the vector magnetic field at nearly constant altitude (370–438 km) and fixed (2 a.m. to 2 p.m.) local time. The spacecraft has been in a nearly circular polar orbit ("mapping phase") since the beginning of March 1999. Each mapping orbit crosses the equator 28.6° westward of the previous orbit. We acquire global coverage of the planet with track-to-track separation of ≈1° (59 km separation) at the equator every 28 days. Subsequent 28-day cycles "fill in the gaps" and provide, at the end of 1 Mars year, ground tracks crossing the equator every 3 km. The magnetic field map presented in this report uses observations obtained during two complete Mars years (one Mars year is equivalent to 687 days).

The magnetic field measured at mapping altitude is dominated by sources in the crust (remanent magnetism) and external fields generated by the interaction of Mars' atmosphere with the solar wind. The Mars crust is about an order of magnitude more intensely magnetized than that of Earth (1, 4), producing fields of as much as 220 nT at MGS mapping altitude. The external field is highly variable, reflecting temporal variations of the solar wind at Mars, ranging from a few nT in magnitude to, rarely, as much as ≈100 nT. Typical night side external fields are ≈10 nT in magnitude and approximately randomly distributed in direction with a slight bias in the component directed along the Mars–Sun line (5). A previous map of the three components of the crustal magnetic field (6) was constructed by using night side observations only (minimizing external fields), averaged and decimated along track, and sorted into bins (1° latitude by 1° longitude) from which the median value was extracted as an estimate of the crustal field. The signal fidelity and spatial resolution of this early map was limited by the presence of residual external fields. The map presented here (Fig. 1) benefits from the use of more observations (two complete Mars years) and a more effective means of external field removal (see *Appendix A: Magnetic Field Map*).

Fig. 1 is a global map of ΔB_r, essentially a 360×180-pixel "image" of the filtered radial magnetic field, color contoured over two orders of magnitude variation in signal amplitude. The map is superposed on the Mars Orbiter Laser Altimeter shaded topography map (7), which appears where ΔB_r falls below a threshold value, ± 0.3 nT per degree of latitude (5×10^{-3} nT/km) traversed by MGS. It is important to note that pixel values representing adjacent longitudes are statistically independent, because of the way MGS orbits accumulate global coverage. Wherever more than a few pixels of the same sign (color) appear together, the map accurately reflects spatial variations in crustal magnetization. The threshold chosen for the minimum contour is set well above the noise level, so that little noise appears in the map, and to allow sufficient context imagery. The high signal fidelity apparent in the image, and the wide dynamic range of the mapped field, provides unprecedented spatial resolution for a magnetic survey obtained at satellite altitude (8).

Geologic Interpretation

Fig. 1 shows with striking clarity the lack of magnetization associated with major impact basins (Hellas, Argyre, Isidis, Utopia, and Chryse) and volcanic provinces (Elysium, Olympus Mons, Tharsis Montes, and Alba Patera) attributed to erasure of a preexisting magnetic imprint by large impacts and thermal events (9, 10). This map also shows extensive regions of the northern lowlands with a relatively weak magnetic imprint but otherwise similar to that observed south of the dichotomy boundary, suggesting that much of the northern plains are underlain by older magnetized crust. This is particularly evident in Acidalia, Amazonis, Arcadia, and regions surrounding Chryse and Utopia. The smooth, flat, and relatively crater-free northern lowlands are thought to have experienced sedimentary or volcanic resurfacing in the Hesperian and Amazonian ages. The discovery of faint topographical features ("quasi-circular depressions"), thought to be the vestigial remains of ancient buried
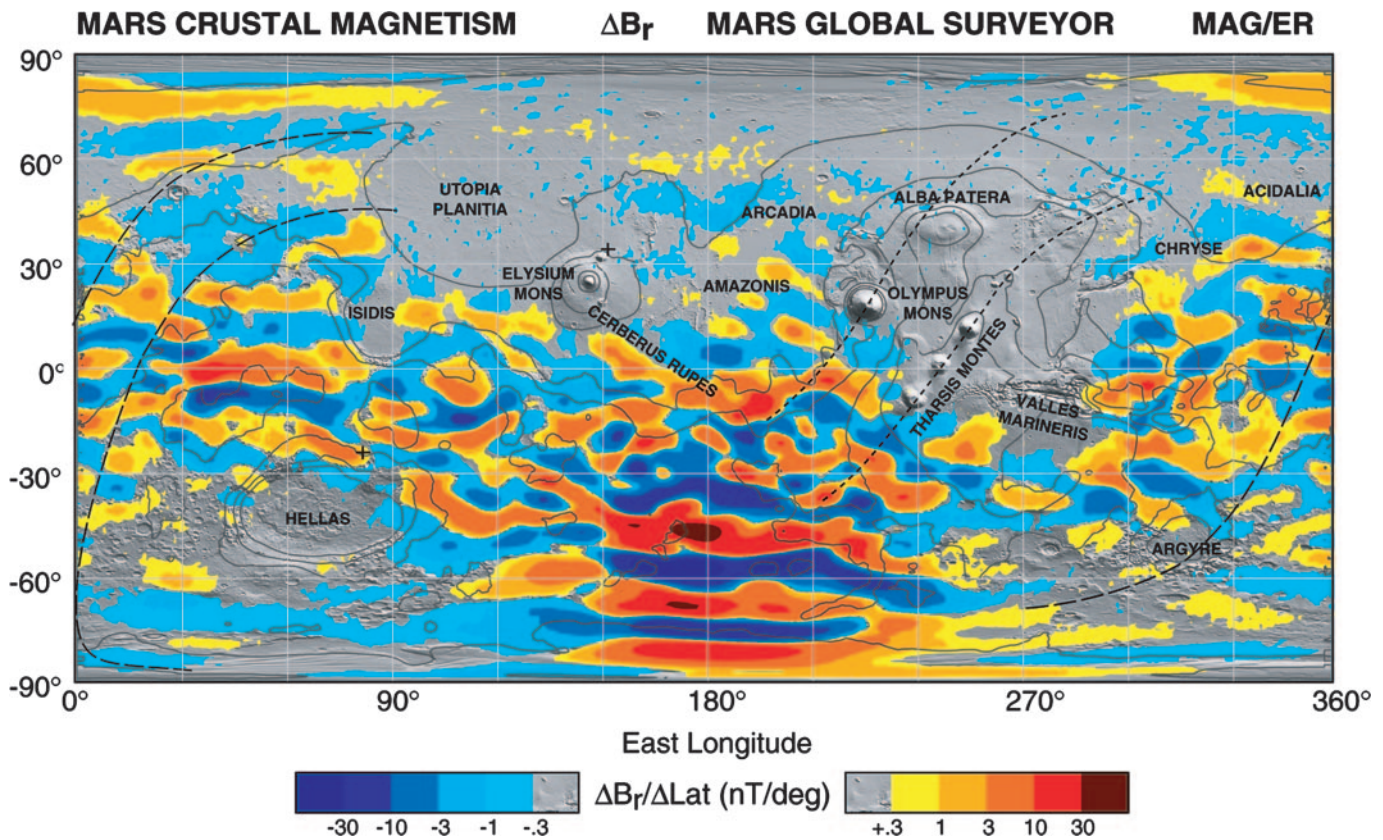

Fig. 1. Map of the magnetic field of Mars observed by the MGS satellite at a nominal 400-km altitude. Each pixel is colored according to the median value of the filtered radial magnetic field component observed within the 1° × 1° latitude/longitude range represented by the pixel. Colors are assigned in 12 steps spanning two orders of magnitude variation. Where the field falls below the minimum contour, a shaded Mars Orbiter Laser Altimeter topography relief map provides context. Contours of constant elevation (−4, −2, 0, 2, and 4 km elevation) are superimposed, as are dashed lines representing rotations about common axes (short dashed line, axis northeast of Elysium Mons; long dashed line, axis northeast of Hellas).

craters (11), throughout the northern lowlands implies that the underlying crust may be as old as the Noachian southern highlands.

Association of Magnetic Features and Known Fault Systems. At least two major faults, previously identified in imagery and topography, align with contours of the magnetic field measured at satellite altitude. Cerberus Rupes is part of an extensive fracture system, Cerberus Fossae, extending from about 12°N, 154°E to 6°N, 175°E, southeast of Elysium (12). The northwest trending fractures and fissure vents of this system separate the Cerberus Plains, a broad, topographically flat expanse of young volcanic flows to the south and southeast, from the older, knobby terrain to the north. The magnetic contours in this region align with fractures of this system and extend for ≈2,000 km or more. Because very large volumes of intensely magnetized rock are required to produce significant fields at a 400-km altitude, this visible feature marks an extensive magnetization contrast (intensity and/or direction of magnetization) aligned with the fracture system. Similar trending magnetic anomalies can be traced, discontinuously, down to mid southern latitudes (−40°).

The magnetic contours along the eastern extent of Valles Marineris align with this fault system as well (positive, or red, contours above and negative, or blue, below). Valles Marineris is a 4,000-km-long system of west–northwest-trending interconnected troughs, linear pit chains, and parallel grabens just south of the equator spanning 250°E to 320°E longitudes (13). The troughs reach depths of 8–10 km below the surrounding plateau and formed subsequent to Lunae and Syria Plana plateaus dating

to the Early Hesperian, ≈3.5 billion years ago (14). The magnetic contours along the eastern extent of Valles Marineris, from about 285°E to 300°E, indicate the presence of a significant contrast in crustal magnetization aligned with the system. The western extent of Valles Marineris is effectively nonmagnetic and flanked by the Syria, Sinai, and Solis Plana to the south and Lunae planum to the north. The transition to magnetized crust moving eastward along Valles Marineris roughly coincides with the transition from ridged plains terrain, both north and south, to the more heavily cratered, ostensibly older terrain to the east (e.g., Lunae Planum to Xanthe Terra). This observation suggests erasure of a preexisting magnetic imprint associated with the encroachment of volcanic flows, moving eastward, with somewhat greater effectiveness southward of Valles Marineris where more material was emplaced. Magnetized crust can be effectively demagnetized over geologic time by thermal remagnetization in a weak field environment at elevated temperatures (see *Appendix B: Thermal Remagnetization*). The efficacy of demagnetization depends critically on the magnetic mineralogy in the crust and both the duration and temperature of the thermal event.

Association of Magnetic Features and Volcanic Constructs. The crustal magnetic fields mapped to the north, west, and south of Olympus Mons offer further evidence of thermal demagnetization by the emplacement of thick volcanic flows atop a previously magnetized crust. Magnetic contours in Arcadia and Amazonis extend inward toward Olympus Mons no further than approximately the −2 km elevation contour marking the extension of the aureole some 1,000 km to the north and northwest. Similarly,

magnetic contours mapped in the vicinity of Elysium Mons do not penetrate beyond the -2 km elevation contour that encircles that volcanic construct. Both of these constructs are massive enough to significantly load the lithosphere, and both have emplaced volcanic flows of many kilometers thickness in their vicinity. Volcanism on Mars is characterized by high rates of effusion (15) that would be required to heat large volumes of crust beneath volcanic flows.

Significant magnetic fields *are* observed above volcanic provinces in the southern highlands, particularly Syrtis Major west of the Isidis basin and Hesperia Planum to the northeast of Hellas. A diminution of the field near the summit of Hesperia (20.5°S and 104.5°E) suggests that these flows have only partially demagnetized the underlying crust. These low relief volcanic constructs have emplaced $\approx 1/2$ to 1 km of flows atop the crust (16) and are thin compared with those in Tharsis and Alba Patera. These flows are thought to be flood lavas extruded at extremely high rates, emplaced in a high volume, single-cooling unit of great extent (15). The partial demagnetization associated with Hesperia, combined with the nearly complete demagnetization associated with Tharsis and surrounding volcanism, suggests that crustal magnetization is borne in a layer a few kilometers thick. Likewise, the northern lowlands may have experienced a catastrophic volcanic flooding event in the Hesperian, burying the crust to a depth of ≈ 1 km or more (17). Such an event could appreciably diminish the magnetic signature of the underlying crust if the magnetized layer was relatively thin (a few kilometers) and if the magnetic mineralogy of the carrier was susceptible to low temperature remagnetization, e.g., magnetite. Note that a succession of relatively thin flows cannot appreciably heat the crust below, because they cool too quickly. To heat an appreciable volume of crust, the flows must be emplaced as a single-cooling unit, e.g., in a span of time that is short compared with the diffusive time constant of the layer(s). This emplacement is consistent with photogeological and topographical analyses (15, 17).

Identification of Great Faults. Another kind of fault, not previously recognized in imagery or topography, can be identified in Meridiani (Fig. 2) by inspection of the magnetic contours. Two dashed lines on the map identify the location of two proposed faults, along which the magnetic field pattern appears to shift. These lines are drawn by rotation of a radius vector about a common axis of rotation identified by a pole (marked with a cross) located at 23°S and 80.5°E, just north of the Hellas basin. The magnetic imprint appears best preserved in the vicinity of 0° latitude and 0° longitude, where the map shows a series of east–west trending features of alternating polarity extending from about 15°N to 30°S, between the two dashed lines. A similar pattern can be found on either side of the proposed fault lines if one allows for a variable displacement along the fault. It appears that the magnetic imprint has been altered in places where the crust has been reworked by impacts (e.g., near 18°S and 331°E, where the large multiring crater Ladon can be identified) and perhaps other events. However, a coherent, if imperfect, pattern remains over much of the crust between 15°N and 30°S in the vicinity of the faults. The two proposed parallel great faults are separated by $\approx 1,400$ km, and a similar pattern in the magnetic field can be traced along both sides of the easternmost fault along $\approx 2,700$ km of its length.

Fig. 3 compares the field sampled along the central meridian, between the two proposed great faults, with that observed $\approx 1,200$ km to the east (E) and west (W) of the pair of faults. This comparison allows for a northward shift (4° latitude, or 240 km) of the pattern west of the faults and linear scaling of the pattern to the east. With the exception of the region near 18°S, all three magnetic profiles agree well. Because the intensity of magnetization of crustal rocks depends critically on details of mineralogy
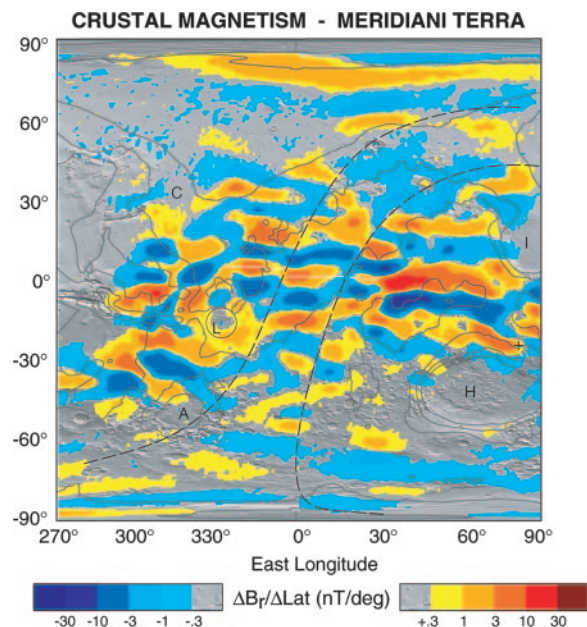

CRUSTAL MAGNETISM - MERIDIANI TERRA

Fig. 2. Magnetic field map of Terra Meridiani, as in Fig. 1 but centered on the zero meridian. Dashed lines indicate parallel great faults drawn as small circles about a common rotation axis ($+$) intersecting the sphere northeast of Hellas (23°S, 83.5°E). The white line marks an axis of symmetry with respect to the magnetic field.

and magnetic microstructure, which might vary over great distances, we do not expect the amplitudes to agree precisely.

Returning to Fig. 2, we note that magnetic contours in the central section between the faults are shifted northward above 0° latitude and southward below 0° latitude relative to those to the east. This characteristic distinguishes a strike-slip fault from a transform fault. A simple strike-slip fault results in a relative displacement of magnetic contours on either side of the fault in
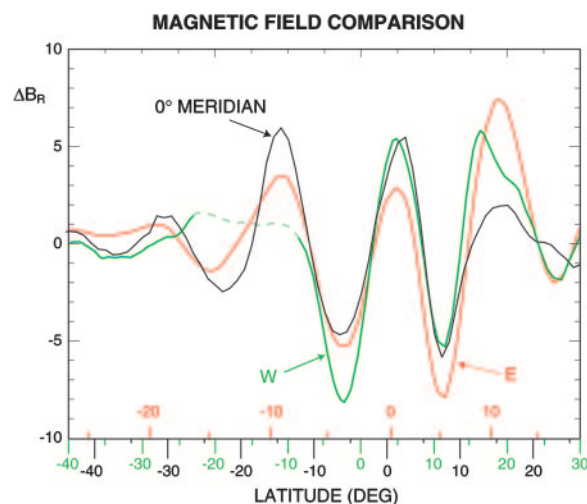

MAGNETIC FIELD COMPARISON

Fig. 3. Magnetic field as a function of latitude along the central meridian (black) compared with that along profiles to the west (green) and east (red) of the two proposed faults. The west curve has been shifted toward the south by 4°, and the east curve has been translated northward by 1° and rescaled as indicated along the horizontal axis. The dashed portion of the west curve indicates the latitude range over which the magnetic imprint was altered by the impact responsible for the multiring crater Ladon. The easternmost profile was taken along a small circle parallel to and eastward of the fault to avoid crossing the proposed fault.
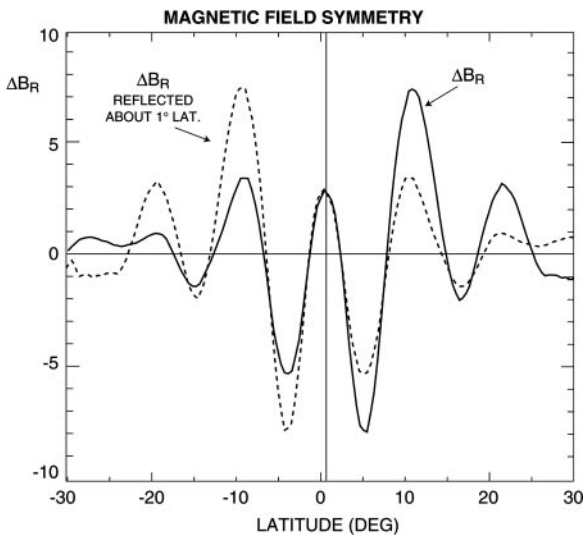
MAGNETIC FIELD SYMMETRY

Fig. 4. Magnetic field as a function of latitude along a small circle to the east of the proposed faults (solid line) and replotted after adjustment of the horizontal scale (5%) and reflection about 1°N (dashed line).

one direction only. Those on either side of the easternmost fault can be aligned only if we allow a change in sign of the relative displacement above and below the putative axis (white line). The change in sign of the relative displacement can be explained, in the context of plate tectonics, with a different spreading rate for the crust on either side of the easternmost fault. The magnetic field along this profile is consistent with symmetry about the ridge axis, at 1° latitude (Fig. 4), allowing for variations in amplitude, as would be expected if this positive magnetic contour aligned with a ridge axis or spreading center.

Plate Tectonics Hypothesis

The magnetic imprint in Meridiani is consistent with that expected of crust formed by plate tectonics in the presence of a reversing dynamo. The essential characteristics of crust formed in this manner are (*i*) a magnetic imprint aligned with the ridge axis or spreading center, (*ii*) a comparable magnetic imprint observed at widely separated locations, and (*iii*) the presence of transform faults, or great faults, along which relative plate motion has occurred. The relative motion of two rigid plates on the surface of a sphere may be described as a rotation about an axis. If two plates have as common boundaries a number of great faults, they must lie on small circles about a common axis. The theory of plate tectonics on Earth was greatly advanced when Morgan demonstrated that the great faults in the Pacific and mid-Atlantic plates lie along such small circles (18). The Pacific plate is spanned by a series of great faults, separated by ≈1,300 km (≈10° latitude) and nearly coincident with coaxial small circles (the Chinook, Mendocino, Murray, Molokai, Clarion, Clipperton, Galapagos, and Marquesas faults). The East Pacific Rise is offset along each of these faults by a few hundred kilometers (typically 500 km). The great faults in Meridiani are consistent with the properties of transform faults and define an axis of rotation (23°S and 80.5°E) describing the relative motion of two plates, north and south of the equator. The separation of the faults (1,200 km) and offset of the putative ridge axis (≈240 km) in Meridiani are comparable with what is observed along ocean ridges on Earth. This similarity is to be expected if transform faults are contraction cracks that relieve the thermal stresses in the cooling lithosphere (19).

The theory of plate tectonics is based on the movement of rigid plates on the planet's surface. Plates are bounded by a ridge,

where new crust is created, a trench or subduction zone, where the crust is consumed, and transform faults, along which plates slip (20). On Earth, seismic observations and sites of recent volcanic activity delineate the edges of plates and trace the downward path of plates in subduction zones (21). Bathymetry and topography provided early clues on plate motions, spreading centers, and trenches; magnetic profiles over spreading centers (2, 22) and the magnetic reversal history of the dynamo (23) could be used to reconstruct plate motions worldwide. The Earth's continued plate motions make it relatively easy to recognize plate tectonics. If plate tectonics did occur on Mars, it has been dormant for billions of years. The crust has been eroded, reworked by large impacts, and largely resurfaced, obscuring topographical clues. If an era of plate tectonics existed early in Mars history, what might remain today as evidence of that era?

Integration of Major Geologic Features Within the Framework of Plate Tectonics

We might expect to decipher some of that history by examination of the magnetic record, where it survives. The magnitude of displacements along transform faults is such that they are observable on Mars from orbital altitude (recognized by an offset in the magnetic imprint) even if individual features (e.g., distinct "magnetic stripes") cannot be resolved. Such offsets provide the best evidence of transform faulting on Earth (19). On Earth, marine surveys allow one to map magnetic anomalies at mid-ocean ridges with a resolution of a few kilometers, well matched to the typical reversal rate of the dynamo (few reversals per million years) and typical spreading rates (few centimeters per year). It is important to recognize that the essential features of the magnetic field above mid-ocean ridges would be observable (apart from the difficulty of measuring small-amplitude signals in the presence of the Earth's much larger main dipole field and ionospheric disturbances) as long as the altitude of observation is small compared with the characteristic scale of the ridge (linear dimension along the ridge). Quasi-parallel magnetic lineations would be observed, greatly attenuated and with a characteristic wavelength comparable to the altitude of observation; symmetry about the ridge axis would be preserved; and well separated great faults (like those spanning the Pacific plate) could be detected from altitudes less than the separation between them. This follows from a general consideration of the upward continuation of a potential field and has been demonstrated by Purucker and Dyment (24).

We might also expect to find clues among geologic formations that survived to the present. Indeed, Sleep (25) has argued that the stepwise linear sequence of escarpments along much of the dichotomy boundary (separating the northern lowlands and southern highlands) is a series of ridge/transform fault segments. This is particularly evident along the dichotomy boundary south of Elysium Planitia and Amazonis spanning the Isidis Basin and Tharsis. Topography along much of the dichotomy boundary is similar to that seen along passive margins on Earth (25).

We do not here attempt a detailed reconstruction of plate motions on Mars. We wish to draw attention to several prominent geological features that may be relevant to proposed plate motions. The origin of the great Valles Marineris fault system is controversial (13), but it has been attributed to planetary rifting (26–28), and compared with terrestrial plate tectonic rifts, e.g., the east African rift zone. A rift structure of parallel grabens and troughs forms, often along an arc, where the crust is being pulled apart in response to tensile forces. Valles Marineris is oriented nearly perpendicular to the direction of plate motion implied by the two proposed great faults in Meridiani (relative plate motion occurs along the strike of transform faults). Thus, the direction of the tensile forces required to form Valles Marineris, if it is

GEOPHYSICS

indeed a rift structure, is consistent with the motions implied by the proposed transform faults in Meridiani.

The great volcanic edifices of Tharsis (Arsia Mons, Pavonis Mons, Ascraeus Mons, extended to include Ceraunius Tholus/ Uranius Patera and volcanic cones in Tempe Terra) and the pair Olympus Mons–Alba Patera lie nearly on two small circles (Fig. 1, short dashed lines) about a common axis (through 35.5°N and 152°E). The motion of a single plate (Tharsis plate) over a pair of mantle hotspots could form a chain of volcanoes if the magma source periodically breached the crust. The Hawaii–Emperor island chain of volcanoes and seamounts in the Pacific is thought to record the motion of the Pacific plate relative to the mantle (29–31). However, the Mars volcanoes dwarf their terrestrial counterparts in size, are further apart, and likely record many episodes of activity spanning Mars history, from the Noachian, or most ancient, era through the present (32). The relative ages are consistent with plate motion northward over the mantle, with Alba Patera and Uranius Patera forming early and Olympus Mons and Arsia Mons forming later.

Summary and Conclusions

The discovery of magnetic lineations in the southern highlands (1), reminiscent of those observed over ocean ridges on Earth (2), led to the suggestion that Mars experienced an early era of plate tectonics during which the crust formed by sea-floor spreading in the presence of a reversing dynamo. The magnetic field in Meridiani has characteristics unique to plate tectonics: transform faulting, symmetry about a ridge axis, and coherence over great distances. This new evidence supports the notion that the crust of Mars is an assemblage of distinct plates, formed by crustal spreading in the presence of a reversing dynamo, like the Earth's oceanic crust.

The prevailing view of Mars evolution is dominated by the concept of stagnant lid convection (33, 34), in which the planet cools slowly, inefficiently, by conduction through a gradually thickening lithosphere. The consequences of an early era of plate tectonics are profound (35), if not easily reconciled with expectations of crust production and early mantle differentiation (36). Plate tectonics cools the interior quickly, drives convection in the core, and encourages the generation of a planetary magnetic field by dynamo action. Indeed, the demise of the dynamo fairly early in Mars evolution may be related to the cessation of plate tectonics and its effects on heat transfer at the core (35). An early era of plate tectonics on Mars may have come to a halt as a natural consequence of the growth of the southern highlands crust (37). The thick southern highlands crust acts as an insulating lid, increasing mantle temperatures and shutting down plate tectonics when it grows in size beyond a critical fraction (0.5) of the planet's surface.

Appendix A: Magnetic Field Map

Map Construction. Magnetic fields generated by the solar wind interaction are greater in magnitude near the subsolar point and much smaller over the darkened hemisphere. They are also global in spatial scale and therefore highly correlated along track. Components of the magnetic field measured on repeat passes over the same location often appear similar, differing only by a constant offset or long wavelength component attributable to the external field. The map was constructed by using night side observations of the radial field component (Br), averaged and decimated along track, producing a time series of Br sampled once every degree latitude traversed by MGS. We then applied a differentiating filter (three-point Lanczos nonrecursive) to the radial field component series, attenuating low-frequency signals associated with large spatial scales, and sorted into bins (1° latitude by 1° longitude) from which the median value was extracted as an estimate of the crustal field.

The median value of this quantity (ΔBr) is an estimate of the

change in the radial magnetic field along track, approximately in the theta direction, as the spacecraft traverses 1° of latitude. ΔBr is relatively insensitive to external fields and closely related to the theta component of the field (see below). The resulting map has about an order of magnitude increased sensitivity to variations in crustal magnetization.

ΔBr. The components of the vector field $(B_r, B_\theta, B_\varphi)$ may be obtained from the gradient of a scalar potential function, V, represented by a spherical harmonic expansion:

$$V = a \sum_{n=1}^{\infty} (a/r)^{n+1} \sum_{m=0}^{n} P_n^m(\cos \theta)[g_n^m \cos (m\varphi) + h_n^m \sin(m\varphi)],$$

[1]

where a is the planet radius, θ is colatitude, φ is longitude, and the P_n^m are the associated Legendre functions of degree n and order m with Schmidt normalization. The g_n^m and h_n^m are spherical harmonic coefficients of degree n and order m. The radial component of the field is the directional derivative of the potential in the radial direction, $B_r = -\partial V/\partial r$, and the theta component is the directional derivative of the potential in the theta direction, $B_\theta = -1/r \partial V/\partial \theta$. The quantity ΔBr computed along track closely approximates $\partial B_r/\partial \theta$, which differs from B_θ only by the appearance of an additional factor $-(n + 1)$ in the expansion of B_θ by harmonics of degree n. The crustal fields measured at orbit altitude (h) are characterized by large n, and a fairly narrow range of n. The satellite altitude acts as a filter that removes wavelengths much larger than h (corresponding to small values of n) and wavelengths much smaller than h (corresponding to large values of n). Measured signal amplitudes are greatest at wavelengths comparable with the altitude of observation (e.g., refs. 8 and 38), so we may consider the significant terms in the expansion of ΔBr to be nearly the same as those of an appropriately scaled B_θ. Thus, ΔBr appears much like B_θ, apart from the reversal in sign. This may be verified by comparison of contours in Fig. 1 with those of B_θ from previous maps (6). ΔBr may be regarded as a proxy for B_θ, acquired in a manner that beneficially suppresses unwanted "noise" due to externally generated fields. Satellite studies of Earth's magnetic field often use high-pass filtered component data (39), but we prefer ΔBr as computed here by virtue of its close association with B_θ.

Appendix B: Thermal Remagnetization

Emplacement of a uniform layer of hot lava atop the crust can significantly elevate temperatures beneath to a depth of a few times the layer half-thickness at most by conduction. The temperature increase v beneath an infinite layer is given by

$$v = \frac{1}{2} V \left\{ \text{erf}\left(\frac{1 - x/a}{2 \sqrt{kT/a^2}} \right) + \text{erf}\left(\frac{1 + x/a}{2 \sqrt{kT/a^2}} \right) \right\}, \quad [2]$$

where a is the layer half-thickness, V is the layer initial temperature, k is the diffusivity, and t is time (40). This approximation is used for an intrusion into the crust and is intended as an illustration only. For a dimensionless time $\tau = kt/a^2 = 4$, and initial temperature $V = 1,200°C$, the temperature rise at the contact ($x/a = 1$) will have dropped to ≈300°C, to 261°C at $x/a = 2$, to 193°C at $x/a = 3$, to 125°C at $x/a = 4$, and to 74°C at $x/a = 5$. This temperature is in addition to that associated with the usual increase in temperature with depth (typically 10–20°C/ km) and neglects the latent heat of solidification that acts to further increase temperatures. However, a layer placed atop the crust may be expected to cool more rapidly because heat lost to the atmosphere exceeds that available to heat the crust below. If

the temperature at the top of the layer is held at 0°C, just less than one half-thickness (*a*) of crust will be elevated by ≈260°C as the layer cools. Thus, emplacement of such a layer (as a single event) might be expected to substantially heat the crust to a depth of 1/2 to 1 times the thickness of the layer emplaced. Over sufficiently long time scales (millions of years), thermal demagnetization of some crustal rocks (e.g., magnetite) requires temperatures of only ≈300°C (41). In summary, if we attribute the lack of intense magnetization in the areas associated with young flows to thermal remagnetization, we require the magnetization to be borne in a relatively thin layer, and the magnetic mineralogy susceptible to low temperature demagnetization. In addition to heating by conduction, if the base of the magnetized layer

is determined by the temperature at depth, the emplacement of a layer atop the crust will eventually demagnetize an equivalent layer at the bottom, because of its increased depth below the surface.

1. Connerney, J. E. P., Acuña, M. H., Wasilewski, P., Ness, N. F., Reme, H., Mazelle, C., Vignes, D., Lin, R. P., Mitchell, D. & Cloutier, P. (1999) *Science* **284,** 794–798.
2. Vine, F. J. & Matthews, D. H. (1963) *Nature* **199,** 947–949.
3. Acuña, M. H., Connerney, J. E. P., Wasilewski, P., Lin, R. P., Anderson, K. A., Carlson, C. W., McFadden, J., Curtis, D. W., Reme, H., Cros, A., *et al.* (1992) *J. Geophys. Res.* **97,** 7799–7814.
4. Voorhies, C. V., Sabaka, T. J. & Purucker, M. (2002) *J. Geophys. Res.* **107,** 10.1029/2001JE001534.
5. Ferguson, B. B., Cain, J. C., Crider, D. H., Brain, D. A. & Harnett, E. M. (2005) *Geophys. Res. Lett.*, in press.
6. Connerney, J. E. P., Acuña, M. H., Wasilewski, P., Kletetschka, G., Ness, N. F., Reme, H., Lin, R. P. & Mitchell, D. (2001) *Geophys. Res. Lett.* **28,** 4015–4018.
7. Smith, D. E., Zuber, M. T., Solomon, S. C., Phillips, R. J., Head, J. W., Garvin, J. B., Banerdt, W. B., Muhleman, D. O., Pettengill, G. H., Neumann, G. A., *et al.* (1999) *Science* **284,** 1495–1503.
8. Connerney, J. E. P., Acuña, M. H., Ness, N. F., Spohn, T. & Schubert, G. (2004) *Space Sci. Rev.* **111,** 1–32.
9. Acuña, M. H., Connerney, J. E. P., Ness, N. F., Lin, R. P., Mitchell, D., Carlson, C. W., McFadden, J., Anderson, K. A., Reme, H., Mazelle, C., *et al.* (1999) *Science* **284,** 790–793.
10. Acuña, M. H., Connerney, J. E. P., Wasilewski, P., Lin, R. P., Mitchell, D., Anderson, K. A., Carlson, C. W., McFadden, J., Reme, H., Mazelle, C., *et al.* (2001) *J. Geophys. Res.* **106,** 23403–23417.
11. Frey, H. V., Roark, J. H., Shockey, K. M., Frey, E. L. & Sakimoto, S. E. H. (2002) *Geophys. Res. Lett.* **29,** 10.1029/2001GL013832.
12. Plescia, J. B. (2003) *Icarus* **164,** 79–95.
13. Lucchitta, B. K., McEwen, A. S., Clow, G. D., Geissler, P. E., Singer, R. B., Schultz, R. A. & Squires, S. W. (1992) in *Mars*, eds. Kieffer, H., Jakosky, B. M., Snyder, C. W. & Matthews, M. S. (Univ. of Arizona Press, Tucson), pp. 453–492.
14. Tanaka, K. L. (1986) *J. Geophys. Res. Suppl.* **91,** E139–E158.
15. Greeley, R. & Spudis, P. D. (1981) *Revs. Geophys. Space Phys.* **19,** 13–41.
16. Hiesinger, H. & Head, J. W., III (2004) *J. Geophys. Res.* **109,** 10.1029/2003JE002143.
17. Head, J. W., III, Kreslavsky, M. A. & Pratt, S. (2002) *J. Geophys. Res.* **107,** 10.1029/2000JE001445.
18. Morgan, W. J. (1968) *J. Geophys. Res.* **73,** 1959–1982.
19. Turcotte, D. L. (1974) *J. Geophys. Res.* **79,** 2573–2577.
20. Wilson, J. T. (1965) *Nature* **207,** 343–347.
21. Isacks, B., Oliver, J. & Sykes, L. R. (1968) *J. Geophys. Res.* **73,** 5855–5899.
22. Pittman Spaceiiiqq, W. C. & Heirtzler, J. R. (1966) *Science* **154,** 1164–1171.
23. Vine, F. J. (1966) *Science* **154,** 1405–1415.
24. Purucker, M. E. & Dyment, J. (2000) *Geophys. Res. Lett.* **27,** 2765–2768.
25. Sleep, N. H. (1994) *J. Geophys. Res.* **99,** 5639–5655.
26. Hartmann, W. K. (1973) *Icarus* **19,** 550–575.
27. Blasius, K. R., Cutts, J. A., Guest, J. E. & Marsursky, H. (1977) *J. Geophys. Res.* **82,** 4067–4091.
28. Frey, H. V. (1979) *Icarus* **37,** 142–155.
29. Wilson, J. T. (1963) *Can. J. Phys.* **41,** 863–870.
30. Morgan, W. J. (1971) *Nature* **202,** 42–43.
31. Sleep, N. H. (1990) *J. Geophys. Res.* **95,** 6715–6736.
32. Tanaka, K. L., Scott, D. H. & Greeley, R. (1992) in *Mars*, eds. Kieffer, H., Jakosky, B. M., Snyder, C. W. & Matthews, M. S. (Univ. of Arizona Press, Tucson), pp. 345–382.
33. Schubert, G., Solomon, S. C., Turcotte, D. L., Drake, M. J. & Sleep, N. H. (1992) in *Mars*, eds. Kieffer, H., Jakosky, B. M., Snyder, C. W. & Matthews, M. S. (Univ. of Arizona Press, Tucson), pp. 147–183.
34. Hauck, S. A., II, & Phillips, R. J. (2002) *J. Geophys. Res.* **107,** 10.1029/2001JE001801.
35. Nimmo, F. & Stevenson, D. J. (2000) *J. Geophys. Res.* **105,** 11969–11979.
36. Breuer, D. & Spohn, T. (2003) *J. Geophys. Res.* **108,** 10.1029/2002JE001999.
37. Lenardic, A., Nimmo, F. & Moresi, L. (2004) *J. Geophys. Res.* **109,** 10.1029/2003JE002172.
38. Blakely, R. J. (1995) *Potential Theory in Gravity and Magnetic Applications* (Cambridge Univ. Press, Cambridge, U.K.).
39. Langel, R. A. & Hinze, W. J. (1998) *The Magnetic Field of the Earth's Lithosphere* (Cambridge Univ. Press, Cambridge, U.K.).
40. Carslaw, H. S. & Jaeger, J. C. (1959) *Conduction of Heat in Solids* (Oxford Univ. Press, London), pp. 54–55.
41. Dunlop, D. J. & Ozdemir, O. (1997) *Rock Magnetism: Fundamentals and Frontiers* (Cambridge Univ. Press, Cambridge, U.K.).

GEOPHYSICS